

Review

# Current Concepts in Multi-Modality Imaging of Solid Tumor Angiogenesis

Moataz A. Soliman <sup>1</sup>, Jeffrey Guccione <sup>2</sup>, Anna M. Reiter <sup>3</sup>, Ahmed W. Moawad <sup>4</sup> , Ashley Etchison <sup>5</sup>, Serageldin Kamel <sup>6</sup>, Aline D. Khatchikian <sup>7</sup>  and Khaled M. Elsayes <sup>4,\*</sup>

<sup>1</sup> Department of Diagnostic Radiology, Northwestern University, Evanston, IL 60201, USA; moataz.a.soliman@students.kasralainy.edu.eg

<sup>2</sup> Department of Diagnostic and Interventional Imaging, The University of Texas Health Sciences Center at Houston, Houston, TX 77030, USA; jeffrey.Guccione@uth.tmc.edu

<sup>3</sup> School of Medicine, University of Texas Southwestern, Dallas, TX 75390, USA; anna.Reiter@UTSouthwestern.edu

<sup>4</sup> Department of Diagnostic Radiology, The University of Texas M. D. Anderson Cancer Center, Houston, TX 77030, USA; ahmedw.moawad@mercyhealth.org

<sup>5</sup> Department of Diagnostic Radiology, Baylor College of Medicine, Houston, TX 76798, USA; ashley.Etchison@bcm.edu

<sup>6</sup> Department of Lymphoma and Myeloma, The University of Texas M. D. Anderson Cancer Center, Houston, TX 77030, USA; skattia@mdanderson.org

<sup>7</sup> Department of Diagnostic Radiology, McGill University, Montreal, QC H3G 1A4, Canada; aline.d.khatchikian@mail.mcgill.ca

\* Correspondence: kmelsayes@mdanderson.org

Received: 28 September 2020; Accepted: 19 October 2020; Published: 3 November 2020



**Simple Summary:** The recent increase in the use of targeted molecular therapy including anti-angiogenetic agents in cancer treatment necessitate the use of robust tools to assess and guide treatment. Angiogenesis, the formation of new disorganized blood vessels, is used by tumor cells to grow and spread using different mechanisms that could be targeted by anti-angiogenetic agents. In this review, we discuss the biological principles of tumor angiogenesis and the imaging modalities that could provide information beyond gross tumor size and morphology to capture the efficacy of anti-angiogenetic therapeutic response.

**Abstract:** There have been rapid advancements in cancer treatment in recent years, including targeted molecular therapy and the emergence of anti-angiogenic agents, which necessitate the need to quickly and accurately assess treatment response. The ideal tool is robust and non-invasive so that the treatment can be rapidly adjusted or discontinued based on efficacy. Since targeted therapies primarily affect tumor angiogenesis, morphological assessment based on tumor size alone may be insufficient, and other imaging modalities and features may be more helpful in assessing response. This review aims to discuss the biological principles of tumor angiogenesis and the multi-modality imaging evaluation of anti-angiogenic therapeutic responses.

**Keywords:** cancer imaging; anti-angiogenic therapy; treatment response; angiogenesis

## 1. Introduction

In the early 1970s, researchers first proposed that tumor growth is limited by an adequate blood supply. This concept propagated investigative research to explore various angiogenic factors, including the discovery of the human vascular endothelial growth factor (VEGF) in the 1980s. Eventually, researchers translated their growing knowledge about angiogenesis to clinical medicine

by introducing angiogenesis inhibitors as a therapy for angiogenic diseases [1,2]. Due to the unique relationship between VEGF and malignant neovascularization, VEGF became the principal target of interest for anti-angiogenic drugs for cancer therapies. Introduced in 2004, bevacizumab, a human monoclonal antibody to VEGF, was the first such agent to receive FDA clearance. Initially, this drug was specifically approved for the treatment of colorectal cancer but has since received FDA approval for non-small cell lung cancer, renal cell carcinoma, and glioblastoma. Since then, many such drugs have followed suit and received approval, both monoclonal antibodies to VEGF and treatments which target other pathways. These treatments have impacted numerous other malignancies, including pancreatic neuroendocrine tumors, medullary thyroid cancer, and hepatocellular carcinoma [3].

The non-cytotoxic nature of anti-angiogenic drugs provides a therapeutic advantage over many traditional chemotherapy agents, which generally target disruption of cellular mitosis in both healthy and cancerous cells. However, a relative disadvantage of anti-angiogenic drug use is difficulty in determining the most effective dose and treatment duration since optimal regimens are difficult to establish [1]. Unfortunately, the breadth of research dedicated to antiangiogenic therapy is challenged by the emergence of drug resistance, specifically with the use of monotherapies. However, recent studies suggest that anti-angiogenic therapy may actually normalize intra-tumoral blood vessels, thus making neo-vasculature more sensitive to cytotoxic chemotherapy [4].

Since 1980, imaging has played an important role in the evaluation of tumor angiogenesis in preclinical models [5]. However, there is a wide gap in detection and quantification of angiogenesis between various clinical imaging and microscopic modalities. For example, conventional US, CT, and MRI can provide detailed information about gross tumor size and morphology, in addition to the vascularity pattern of large vessels. However, details about the microvascular environment are limited with these studies. More advanced dynamic imaging techniques, such as CT perfusion, are able to measure blood flow, blood volume, and vascular permeability. However, they are unable to provide specific information about alterations in vasculature and do not directly correlate with changes in vascular permeability, vascular density, or tumoral neo-angiogenesis [6]. Fluorescence-based imaging and electron microscopy are other options which may yield more detailed information about the structure, density, and permeability of the blood vessels. An example is seen in retinal and choroidal imaging, where fluorescent dye exposes leaky capillaries and detects ocular angiogenesis, visible externally through the eye. However, fluorescence imaging has its own limitations; most importantly, it is unable to provide accurate quantitative information [7].

Current research is focused on determining imaging regimens for follow-up of anti-angiogenic therapy. Efforts are also dedicated to improving both imaging diagnostic accuracy and anti-angiogenic interventional therapies [2]. Specifically, the discovery of a validated imaging biomarker will not only facilitate more accurate follow-up of anti-angiogenic therapy but also aid in determining correct therapeutic dose and treatment duration through improved evaluation of biological processes [6,8]. For example, dynamic contrast-enhanced (DCE) MRI with gadolinium-diethylenetriamine-penta-acetic acid (Gd-DPTA) labeled albumin has been found to be a reliable marker in detecting early response to bevacizumab in breast cancer animal models, with measurable reduction of vascular permeability at different doses [9].

## 2. Molecular Basis of Angiogenesis

Under normal physiological conditions, angiogenic factors are strictly controlled by cellular machinery [10]. However, this meticulous management becomes unregulated and disorganized in neoplastic processes. During rapid tumor growth, neoplastic cells must be within millimeters of feeding vessels, as oxygen diffusion is limited to approximately 250  $\mu\text{m}$  [11]. To maintain an adequate blood supply, tumor cells direct host cellular machinery via hypoxia-induced angiogenesis. New blood vessels form when cellular production of angiogenic factors outweighs the manufacture of anti-angiogenic factors (Figure 1) [10,12].

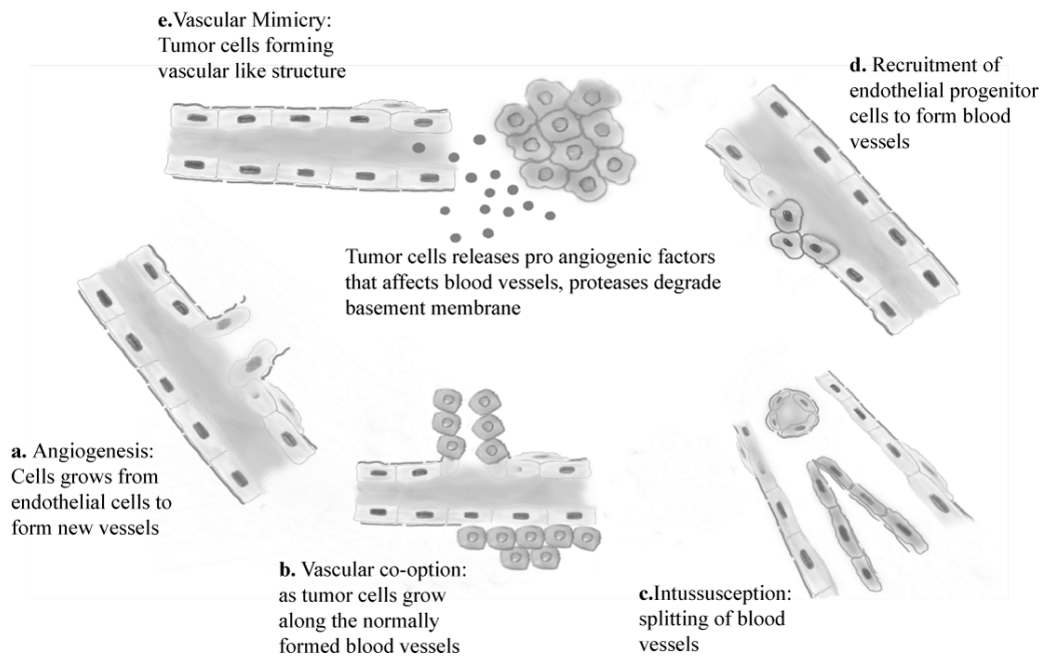


**Figure 1.** Graphic representation of various routes leading to new blood vessel formation within a tumor. (a) Angiogenesis, (b) vascular cooption, (c) intussusception, (d) endothelial progenitor recruitment, (e) vascular mimicry.

Tissue hypoxia stimulates the production of VEGF and fibroblast growth factor (FGF). In response, endothelial cells produce proteases that dissolve cellular basement membranes. This process propagates the formation of vascular buds, which eventually evolve into functional new blood vessels. Subsequent recruitment of accessory cells produce the necessary supporting extracellular matrix for newly formed vessels [2,13].

Although de novo formation of blood vessels, known as neovascularization, commonly occurs in malignancies, additional angiogenic pathways can also result in new vessel formation (Figure 1). These are the same processes that occur in physiologic blood vessel formation and include intussusception, when a single vessel splits into two vessels without cellular mitosis, and vascular mimicry, whereby tubular vessel-like structures form [14]. Tumor stem cells can also differentiate directly into endothelial cells, which begins new vessel formation [8].

Angiogenesis is governed by multiple angiogenic factors that may represent targets for novel molecular-based therapies. Some of these angiogenic elements include hypoxia-induced factors, growth factors, VEGF, platelet-derived growth factors, FGF2, matrix metalloproteinases,  $\alpha v \beta 3$  integrin, and E-selectin [14]. Among these, VEGF is considered the most important angiogenic factor in the formation of new blood vessels [15]. Unlike other growth factors such as fibroblast growth factor (FGF) that stimulates mitosis in multiple cell lineages, VEGF is specific for stimulating vascular endothelial cells and thus angiogenesis [16].

Many architectural and functional differences exist between vessels formed under physiologic and neoplastic conditions. For example, tumoral angiogenesis results in the rapid overproduction of angiogenic factors, which makes newly formed blood vessels often disorganized and highly permeable to macromolecules [17–19]. Vascular endothelial cadherin is crucial for maintaining cell–cell junctions, thus maintaining vascular integrity. VEGF activates the intracellular signaling pathway that downregulates VE-cadherin molecules, a major contributing factor in increasing vascular permeability [20]. Compared to orderly physiologic vessel formation, tumor vessels may haphazardly course throughout surrounding tissues and branch in atypical patterns [1]. Tumoral vessels, which are often not uniformly distributed across tumor tissue, demonstrate an increased number of blood vessels per unit area, known as microvascular density (MVD). Additionally, disorganized blood vessel

formation can lead to intra-tumoral arteriovenous (AV) shunting. Finally, tumoral angiogenesis can result in blood flow fluxes out of the vascular compartment into the interstitial compartment due to increased oncotic pressure. This oncotic pressure increase is caused by leakage of plasma proteins into the interstitium through weak tumor vessel walls (Figure 2) [17–19].

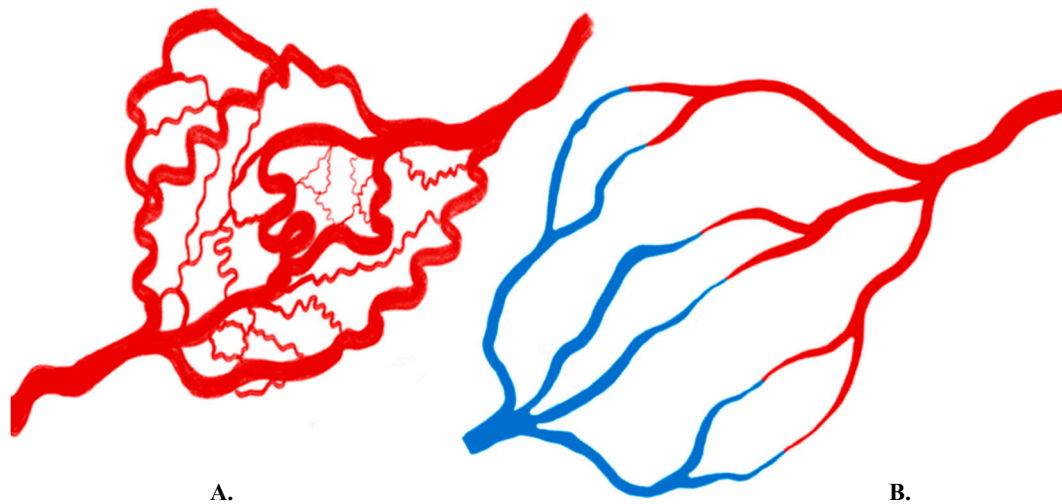


**Figure 2.** (A) Schematic representation of tumor vasculature showing disorganized architecture of the neo-angiogenesis with arteriovenous shunting. (B) Schematic representation of normal vasculature showing well organized arteriovenous capillary formation, red represents oxygenated blood and blue represents deoxygenated blood. (adapted from: Imaging Angiogenesis: Applications and Potential for Drug Development. Janet C. Miller, et al. Journal of the National Cancer Institute, 2005.

Knowledge of the key differences between normal and abnormal vessels assists clinicians with the diagnosis, treatment, and prognosis of various neoplastic processes. The various structural and functional differences between physiologic and tumoral vessels are appreciated with various molecular and non-molecular imaging methods, including cross-sectional imaging and digital subtraction angiography (DSA) (Figure 2).

### 3. Overview of Imaging Angiogenesis

There are two main methods for imaging angiogenesis in tumoral tissue, including structural and functional assessments. Structural or anatomic evaluations involve molecular and non-molecular imaging, which include CT, MRI, contrast-enhanced ultrasound (CEUS), whole body optic imaging (after tumor labeling with green fluorescence), and positron emission tomography (PET) scan [7]. The molecular method relies on intravenous contrast, which contains nanoparticles, to bind specifically to ligands upregulated on the surfaces of neo-angiogenic vessels [21,22]. Conjugating the nanoparticles to surface ligands on actively proliferating endothelial cells bridges morphological imaging techniques and evaluation of angiogenesis at the molecular level [23].

The second method for evaluating angiogenesis focuses on cellular function and involves various perfusion parameters. These factors include blood flow, mean transient time, regional blood volume and assessment of vascular permeability. Vascular permeability is assessed with dynamic contrast-enhanced MRI or CT [21]. This parameter is significantly valuable as it correlates with vascular integrity and pathological grade in some tumors [24,25]. For example, the assessment of vascular permeability using MRI techniques could differentiate various grades of gliomas with high accuracy, particularly when combined with perfusion studies [26].



#### 4. Invasive and Non-Invasive Imaging Methods

Non-invasive imaging methods primarily involve MRI and CT. MRI has various types of contrast agents that can be used. Low-molecular-weight MRI contrast agents, such as the now discontinued gadofosveset trisodium, extravasates at sites of angiogenesis, but also can leak from normal blood vessels. The most commercially used MRI contrast agents are macromolecular, such as Gd-DTPA, and are retained within normal vasculature but leak from vessels formed through a pathologic angiogenesis process, typical of tumors (Figures 3 and 4). Ultrasmall superparamagnetic iron oxides (USPIOs) are high-contrast MRI contrast agents which are very small and are useful in assessment of the blood pool. Currently, they are more frequently utilized in research settings but are helpful in evaluating vessel characteristics, such as size or density [27] (Figure 5).

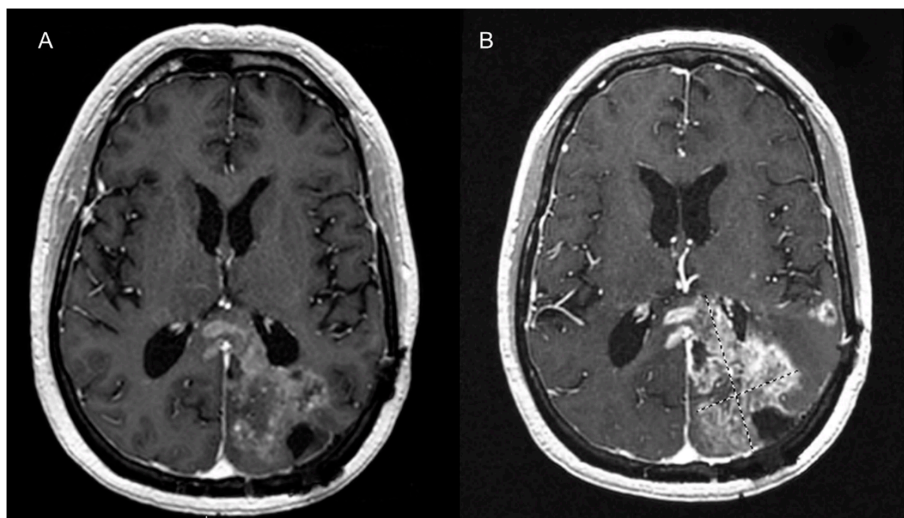


**Figure 3.** T1-weighted contrast-enhanced axial image of the brain with a left occipital glioblastoma. (A) This image shows enhancing local tumoral recurrence, prior to starting anti-angiogenic therapy. (B) Nine months after initiation of anti-angiogenic therapy shows marked reduction of the enhancing component and associated vasogenic edema.

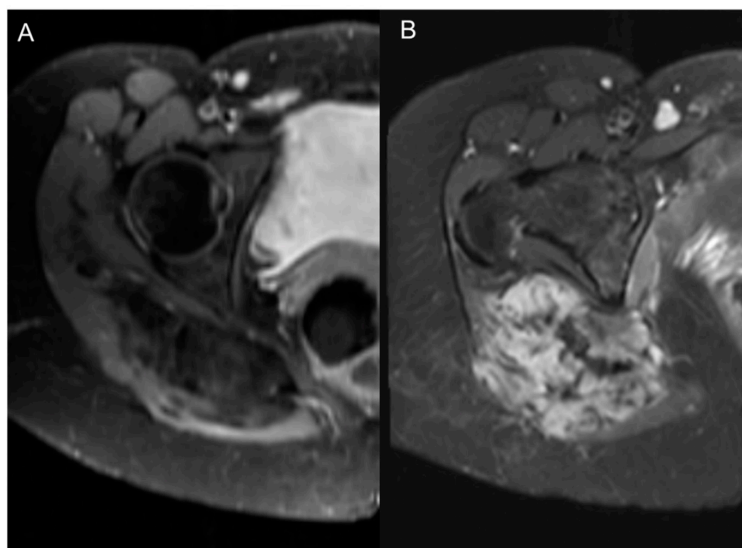


**Figure 4.** Axial T1 fat suppression contrast-enhanced MRI images of the pelvis in a female patient with fibro-desmoid tumor of the gluteal region. (A) Post- and (B) pre-treatment images after initiation of anti-angiogenic therapy.

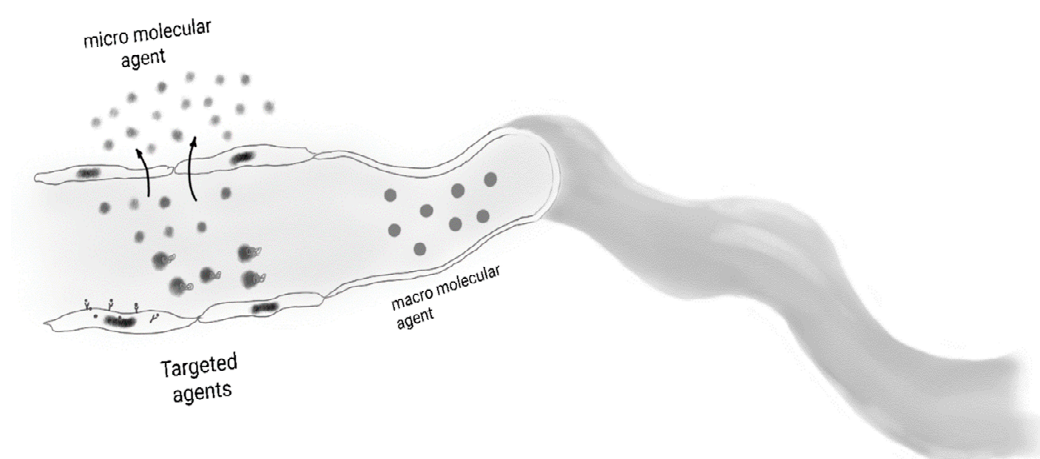


**Figure 5.** Graphic illustrates various contrast medias used in contrast-enhanced MRI, such as ultrasmall superparamagnetic iron oxide (USPIO). The small molecular agents leak through the vessel walls. Macromolecules remain in the vascular compartment. Similarly, ligand-bound contrast material remains in the vascular compartment. Targeted agents are bound to surface target molecules.

However, CT imaging with iodinated contrast is utilized as well, but it introduces ionizing radiation. Ultimately, the decision of CT or MRI is usually made on a case-by-case basis and is often dependent on the region being imaged and institution preference.

Catheter angiography/DSA is a more invasive method where contrast is injected directly in the artery proximal to the tumor. This can be achieved using iodinated contrast agents or carbon dioxide (CO<sub>2</sub>). CO<sub>2</sub> has an advantage as it is not nephrotoxic and does not have the risk of allergic reactions like iodinated contrasts [28]. Regardless, evaluation is typically limited to vessels larger than 250  $\mu\text{m}$  in typical angiography equipment, which makes microvascular assessment impossible [28]. Much like CT, these methods also carry the risk of ionizing radiation [29] (Figure 6).

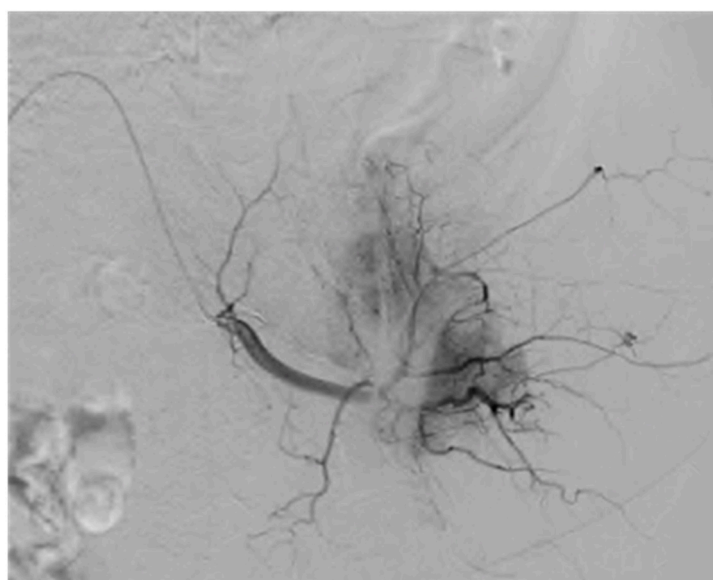


**Figure 6.** Digital subtraction angiography in a case of a metastatic renal carcinoma lesion in the left acetabulum. During the embolization procedure, there is significant tumoral vascular blush, denoting extensive intratumoral vessel formation.

Even more invasive imaging methods quantify tumor microvascular density (MVD), which is an angiogenesis biomarker calculated from pathologic specimens, usually obtained after biopsy. Theoretically, acquisition of multiple biopsies throughout the course of the disease would provide information regarding response to anti-angiogenic therapy. However, MVD values are not entirely reliable because most tumors are not homogeneously vascular [30]. For example, most areas of active angiogenesis are located at a tumor's periphery compared to the less vascularized necrotic core [31].

When comparing techniques, imaging biomarkers may be advantageous over molecular biomarkers as the former is less invasive and has the added benefit of providing global information about tumor heterogeneity [8,32]. Although imaging biomarkers, such as perfusion studies, mean transient time, relative blood volume, and contrast transfer coefficient, are promising parameters for anti-angiogenic treatment response, these biomarkers still require validation in the clinical setting for correlation of imaging findings and treatment response [33].

## 5. Choosing the Best Imaging Modality for Evaluating Angiogenesis

In various clinical trials evaluating angiogenesis, the imaging modality of choice (MRI versus CT) is based on the availability [34]. The volume transfer coefficient ( $K_{trans}$ ) values, which combine both blood flow and vascular permeability surface area product, were comparable between these two modalities [33]. However, many studies that used diagnostic imaging for the evaluation of angiogenesis utilized MRI [35]. Additionally, CT and MRI offer comparable results regarding spatial resolution, although MRI can give information about water diffusion, tissue oxygenation and metabolism, microvascular permeability, and blood flow. PET imaging also appears to be a useful and highly accurate method for the assessment of changes in tumor vascularity [36]. However, its use is somewhat limited due to the lack of widespread availability and poor spatial resolution [17]. Perfusion CT imaging and CEUS are other options which have been utilized for evaluating angiogenesis [37]. Perfusion CT can offer quantitative data about blood flow similar to MRI; however, it carries the risk of exposure to ionizing radiation and also has a poorer signal to noise ratio [19]. With the recent development and advancement of CEUS, it is now possible to evaluate the vascularity of malignant tumors and has shown promise in clinical applications [38]. However, it can be limited in its ability to provide full 3D morphologic details of tumors and presents challenges in anatomically inaccessible regions, such as the retroperitoneum and brain [19].

## 6. Parameters Derived from Imaging Data

### 6.1. Steady-State Imaging

By comparing image intensity before and after the administration of contrast, blood volume at the region of interest can be calculated, which can be used for follow-up of drug therapy. However, a disadvantage of contrast-enhanced MRI and CT is that contrast may leak through the endothelial barrier in disorganized tumoral neo-vasculature, thus yielding inaccurate measures of blood volume. In comparison, microbubble contrast used in CEUS remains within the intravascular compartment and does not leak through vessel walls like traditional contrast agents, and thus is more accurate for measuring blood volume [1].

### 6.2. Dynamic Imaging

A large amount of useful information can be derived from dynamic studies, such as blood volume and blood flow, which may be particularly useful in assessing treatment response and tumor vascular dynamics. Provided that contrast remains within the intravascular compartment during ultrafast imaging techniques, the amount of contrast in each voxel of the image can be tracked and plotted against time such that the area under the curve will correspond to the blood volume [1]. This technique has previously been validated to provide important clinical information. For example, Zhang et al.

demonstrated the prognostic value of regional cerebral blood volume for evaluating treatment response in cases of glioblastoma multiforme [39].

Flow can be calculated in similar ways, and although there are several methods, it generally is a measure of how fast the tracer (contrast) diffuses through a tissue [40]. It also yields a variety of useful parameters (Table 1).

**Table 1.** Summary of the measured and calculated hemodynamic parameters and their clinical significance.

Symbol	Measures	Significance
$C_p$ (arterial concentration)	Concentration of tracer in arterial blood (input function in CT and MRI)	<ul style="list-style-type: none"> <li>Arterial tracer concentration over time</li> <li>Shape of arterial input curve will correspond to the shape of arterial dynamics within the tissue itself</li> </ul>
$C_a$ (arterial concentration)	Concentration of tracer in arterial blood (input function in PET)	(as above)
$F$ (flow)	Blood flow: represents the amount of blood passing per unit of time per tissue mass	Decreased under antiangiogenic therapy
$P$ (permeability)	Capillary wall permeability surface area	Testing the integrity of the blood vessel mesh
$PS$ (permeability-surface area product)	Capillary wall permeability surface area per unit mass of tissue (in practice, $P$ and $PS$ are not clearly separated)	Testing the integrity of the blood vessels mesh in relation to tissue volume
$E$ (extraction fraction)	Extraction fraction of oxygen	Ratio of blood oxygen that a tissue takes up from blood flow
$K_{trans}$ (volume transfer coefficient)	Volume transfer constant from plasma to the extravascular extracellular compartment	<ul style="list-style-type: none"> <li>Predominantly dependent upon tissue perfusion and minorly dependent on permeability and surface area.</li> <li>Decreased with antiangiogenic therapy</li> </ul>
$K_{ep}$ (equilibrium product constant)	Rate constant between the extravascular extracellular compartment and the plasma (efflux of tracer back to the vascular space)	<ul style="list-style-type: none"> <li>Predominantly dependent on vascular permeability and perfusion</li> <li>Variably changed under antiangiogenic therapy</li> </ul>
$K_i$ (net influx rate)	Unidirectional influx constant	
$V_p$ (plasma blood volume)	Fractional blood plasma volume	
$V_a$ (arterial blood volume)	Fractional blood volume	
$V_e$ (extravascular extracellular volume fraction)	Volume of extravascular extravascular per tissue unit volume	

Table 1. Cont.

Symbol	Measures	Significance
IAUC (initial area under the curve)	Area under the curve in contrast concentration against time curve	<ul style="list-style-type: none"> <li>This parameter is affected by perfusion and rBV</li> <li>Decreased under antiangiogenic therapy</li> </ul>
rBV (relative blood volume)	Percentage of blood volume in relation to tissue volume	<ul style="list-style-type: none"> <li>Amount of functional blood vessels within the tumor</li> <li>Changes according to the tumor vascularity</li> <li>Decreases with antiangiogenic therapy</li> </ul>
Perfusion	Amount of blood flow within the capillary system (blood flow rate over organ mass)	<ul style="list-style-type: none"> <li>Tumors will have higher perfusion rather than corresponding normal tissue due to increased microvascular density, larger arterial feeder.</li> <li>Decrease with anti-angiogenic therapy</li> </ul>
MTT (Mean transient time)	Time a contrast agent has to pass through the tissue of interest from the arterial side to the venous draining side (blood volume over blood flow)	<ul style="list-style-type: none"> <li>Correlates with tissue perfusion</li> <li>Decreases with anti-angiogenic therapy</li> </ul>
Vascular permeability	Depends on various parameters like tracer properties, vascular surface area, leakiness and the extracellular extravascular distribution space	Tumors possess immature capillary mesh so are characterized by higher-than-normal vascular permeability

## 7. MR Imaging of Angiogenesis

### 7.1. Unenhanced MRI Imaging of Angiogenesis

Two non-contrast MRI techniques utilized in the evaluation of angiogenesis include arterial spine labeling (ASL) and blood oxygenation level-dependent (BOLD) imaging. ASL is a non-invasive, non-contrast method in which blood is magnetically labeled as it passes towards the organ of interest using RF pulse. The labelled protons interact with the tissue of interest, generating information use to indirectly calculate blood hemodynamics [38]. Using the same principle, ASL is used to generate blood flow maps, such as cerebral blood flow. Similarly, this technique could be used to indirectly evaluate the state of angiogenesis in a tumor (Figure 7) [39].

The applicability of ASL to extracranial tumors is limited due to transient time artifact, such as those produced by patient movement or respiratory motion. Nevertheless, this technique can be extrapolated to assess vascular changes in various extracranial tumors, like renal and ovarian cancers [40,41]. This method is particularly useful in renal cancer patients with renal failure, as no contrast is required. When compared to conventional T1-weighted contrast-enhanced MRI, ASL comparably detects renal cell carcinoma relapses after radiofrequency ablation [42].

The BOLD imaging technique is based on the fact that oxy and de-oxy hemoglobin exhibit different magnetic characteristics. This technique was initially developed for functional brain imaging, yet due to arteriovenous differences in blood oxygenation, indirect calculation of blood flow can be measured. However, it should be noted that this technique is limited by poor spatial resolution and susceptibility artifacts [43].



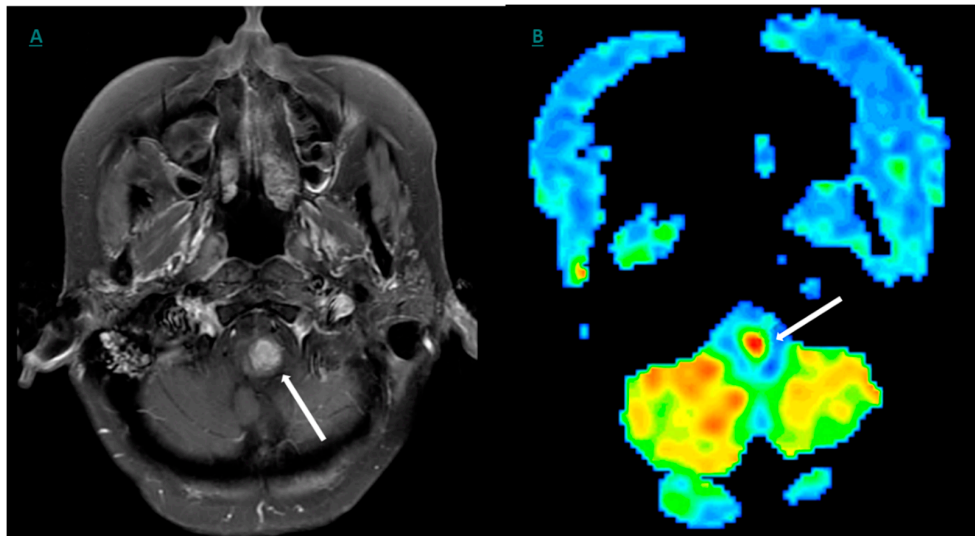


**Figure 7.** (A) DCE MRI axial T1-weighted image showing an enhancing cervicomedullary junction lesion (arrow). (B) The corresponding Arterial Spin Labeling (ASL) showing a relatively increased perfusion in the cervicomedullary junction (arrow).

### 7.2. Contrast-Enhanced MR Imaging of Angiogenesis

Leakage of injected contrast from tumor angiogenic vasculature provides the basis for contrast-enhanced MRI studies. Furthermore, the high spatial resolution of contrast-enhanced MR imaging detects vessels as small as 30–100 micrometers [44]. DCE MRI is based on subjective enhancement curves, which identify angiogenesis in tumoral tissue [45]. It can be performed using either low-molecular-weight (LMW) or high-molecular-weight (HMW) contrast agents [46]. A frequently utilized LMW contrast agent for detection of vascular leakage is albumin-Gd-DTPA, which creates signal enhancement as it leaks into interstitial planes (Figures 5 and 6) [9].

DCE MRI is performed with a T1-weighted technique to determine perfusion parameters and contrast material leakage. On the other hand, a T2\* imaging technique is utilized to calculate cerebral blood flow and is optimized for the assessment of malignancy [47]. In a clinical trial investigating invasive ductal carcinoma, this T2\* imaging technique exhibited a positive correlation between perfusion parameters and microvascular density, especially in larger tumors [45]. Thus, perfusion and DCE MRI techniques can be used to follow-up anti-angiogenic therapy response. Another study, which used colon cancer mouse models treated with bevacizumab, utilized DCE-MRI to assess the maturity and normalization of vessels, while BOLD-MRI was used to evaluate for tumor ischemia and metastatic potential. Using these methods, they concluded that low-dose intermittent treatment with bevacizumab may supplement the use of chemotherapy.

The parameters derived from DCE MRI include the volume of extravascular extracellular space per unit volume, volume of blood plasma per unit volume of tissue, blood vessel permeability, vascular surface area, and interstitial pressure [48,49]. These parameters may be applied to pharmacokinetic studies to evaluate for drug response, tumor recurrence, and progression [48].

### 7.3. Dynamic Susceptibility Contrast (DSC) Perfusion MRI

Dynamic susceptibility contrast (DSC) perfusion MRI, also termed bolus-tracking MRI, depends on the first pass metabolism of the contrast agent in the tissue. This technique involves injecting gadolinium chelate into the vascular compartment and then rapidly acquiring images through the region of interest. As contrast passes through the tissue of interest, the perivascular magnetic field is distorted which leads to T2 de-phasing and loss of signal intensity. When the measured signal intensity is plotted against time, hemodynamic parameters like blood volume and flow are calculated [50].

#### 7.4. Dynamic Contrast-Enhanced Perfusion MRI

With DCE perfusion MRI, T1 shortening is plotted against time. The contrast material diffuses into the extravascular extracellular space in a process dependent on vascular permeability, surface area, and tissue perfusion. By analyzing a specific region of interest, parameters like  $K_{trans}$  and  $V_p$  can be calculated from dynamic contrast-enhanced T1 MRI images (Figure 8) [51].  $V_p$  is a measurement of the fractional plasma volume and is similar to blood volume.  $K_{trans}$  reflects the porosity at the capillary bed and is calculated by the rate that the MRI contrast material accumulates in the interstitial fluid compartment (Figures 8 and 9).

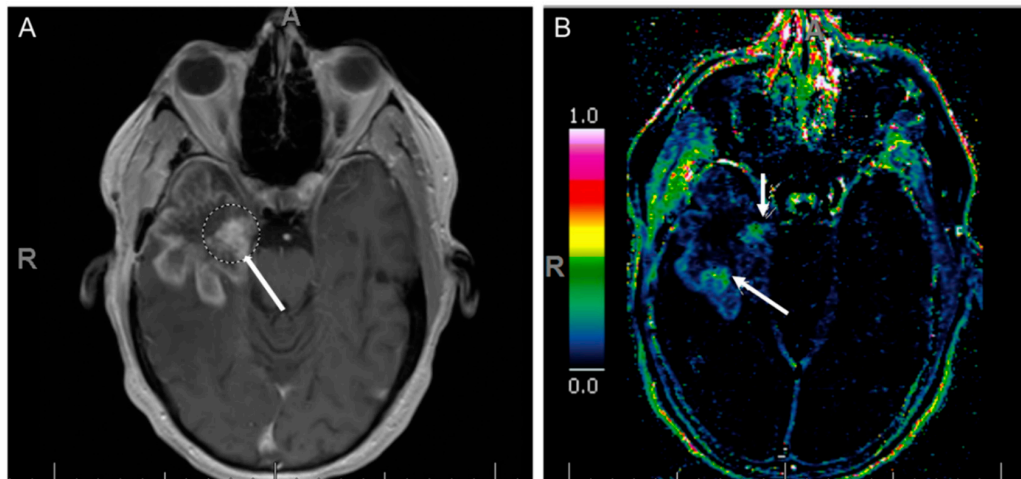


**Figure 8.** A patient with temporal glioblastoma underwent surgical resection followed by radiotherapy. (A) Axial T1 post-contrast image of the brain shows nodular enhancement. (B) This corresponds to  $K_{trans}$  map with increased capillary permeability (arrows). These regions show increased relative cerebral blood flow (rCBF) (not shown), which likely represents recurrence of disease.

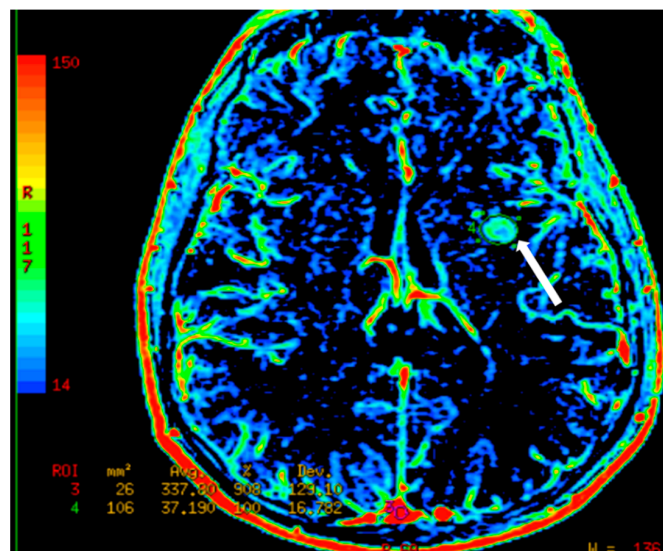


**Figure 9.** Axial dynamic contrast-enhanced (DCE) MRI of the brain with a relative cerebral cerebral blood volume (rCBV) map, which shows relatively increased flow dynamics in the left basal ganglia lesion (arrow).

When a contrast material is injected during dynamic studies, it diffuses through the capillary bed into the extravascular compartment at a rate dependent upon the permeability of the capillary bed and the concentration difference between the plasma and that volume of distribution [52].

## 8. CT Imaging of Angiogenesis

### 8.1. Multi-Slice Computed Tomography (MSCT) Perfusion Imaging Technique

CT imaging is often considered the gold standard for diagnosis, staging, and follow-up of tumors due to its superior spatial resolution with the contrast agents. From contrast-enhanced CT imaging, parameters like vessel size, relative blood volume and three-dimensional anatomy can be derived. However, these parameters represent macroscopic vasculature and fail to provide information at the micro capillary level [53]. Previously, a study determined a positive correlation between malignant breast mass perfusion parameters and increased expression of angiogenic factors where there was over-expression of VEGF and matrix metalloproteinase-2 (MMP-2) [54].

### 8.2. Clinical Applications of CT Perfusion

There are a few significant clinical applications of CT perfusion imaging. Lesion characterization can be achieved by analyzing perfusion values [55]. Previously, it has been shown that differences in perfusion was able to differentiate renal cell carcinoma from oncocytoma. These perfusion differences also extended to differentiate malignant renal tumors from normal renal cortical tissue [56]. Detection of tumoral angiogenesis with CT perfusion imaging is useful in staging tumors, particularly when evaluating perirectal tumors [55]. Additionally, it has been demonstrated to help with detecting nodal metastasis from squamous cell carcinoma and breast cancer (Figure 10) [57,58]. CT perfusion imaging may also predict which patients will respond better to chemo and radiotherapy. This is evidenced by the association between higher blood flow values in tumors which had a more robust treatment response [21]. Finally, some evidence suggests that this technique may also be utilized to detect relapse and evolution of drug resistance [59].

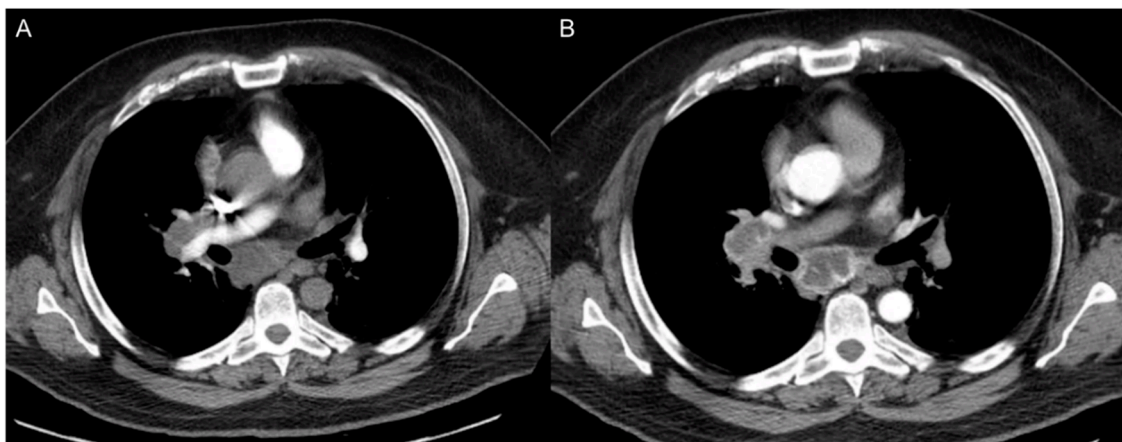


**Figure 10.** CT perfusion of a right hilar lesion was performed following administration of IV contrast. Displayed are selected sequential acquisitions (A,B) collected for measurement of perfusion parameters.

## 9. Ultrasound Imaging of Angiogenesis

The development of high-frequency ultrasound machines permits real-time imaging of angiogenesis with excellent imaging resolution [60]. A combination of power doppler and CEUS quantifies blood flow and characterizes tumoral vascular structures. In experimental models, this combined technique can conduct evaluations for treatment responses to anti-angiogenic drugs [61].

Contrast-enhanced ultrasound uses microbubbles, which are gas filled spheres measuring 1–3  $\mu\text{m}$  surrounded with a single lipid layer. This gas–fluid interface provides an excellent medium for backscattering of ultrasound waves. This happens when the waves interact with injected microbubbles producing nonlinear backscattering. This interaction produces real-time, contrast-specific images that can be viewed side by side with subtracted images. Even at small concentrations, contrast material

can be detected as well as very sluggish flow within the tumor microvasculature [62]. By plotting enhancement versus time, maximal enhancement peak and relative blood volume are calculated. Perfusion is interpreted by the upslope of this curve [63]. The potential utility of microbubble CEUS in evaluating angiogenesis is evident in animal studies. In a study by Sirsi et al., the use of microbubble ultrasound revealed a decreased relative blood volume in tumors after anti-angiogenic therapy. Additionally, these findings correlated with the microvascular density on histological specimens [64].

There have been advances in developing target specific contrast agents. Lipid shells of microbubbles are modified to bind specifically to a transmembrane receptor. The same concept does not apply to soluble proteins (non-membrane-bound proteins) such as matrix metalloproteinase. However, these soluble proteins have to be present in sufficient concentration at the vascular compartment in order to bind to protein specific contrast agents [62].

A similar sonographic technique for evaluating angiogenesis is molecular ultrasound imaging, which uses antibodies bound to the microbubble contrast rather than just altering the lipid shells. These antibodies bind vascular surface receptors, which are over-expressed by many tumors, including vascular endothelial growth factor receptor (VEGFR). When combined with subtracted images, regional areas of target overexpression are revealed. In one study, this method showed a significant reduction of contrast binding after antiangiogenic therapy. The suggestion of this finding is a resultant decreased level of VEGFR expression after therapy and, thus, decreased angiogenic activity in the tumor tissue [65].

## 10. Positron Emission Tomography (PET) and Molecular Imaging

PET imaging is advantageous for patients as the tracers are generally less toxic compared to MRI and CT contrast agents [66]. Additionally, the radiotracers can be conjugated to various substances or ligands, allowing for the ability to target specific receptors or cells. This is often referred to as molecular imaging. For example, radiolabeled VEGF or antiangiogenesis agents can be used in PET to provide evidence that the treatment is targeting the tumor tissue [15]. This imaging technique can also demonstrate the heterogeneity of targeted molecules distributed within the tumor tissue [67]. There are a number of other targets and radiopharmaceuticals that have been studied and utilized, further discussed below (Table 2).

**Table 2.** Molecular targets in molecular imaging of angiogenesis.

Radiolabeled Substance	Example Radiotracer	Tracer Modality *	Significance
VEGF/VEGFR	[ <sup>64</sup> Cu]VEGF <sub>125-136</sub> [68]	PET	<ul style="list-style-type: none"> <li>• VEGF is a significant driver of tumor angiogenesis</li> <li>• VEGFR-2 is upregulated in tumor angiogenesis</li> <li>• Many approved anti-angiogenesis agents target VEGF/VEGFR</li> </ul>
Bevacizumab	<sup>89</sup> Zr-bevacizumab [69]	PET	<ul style="list-style-type: none"> <li>• Bevacizumab targets VEGF-A</li> <li>• Can evaluate biodistribution of treatment</li> <li>• Assesses potential for response prior to treatment</li> </ul>
Integrins ( $\alpha v \beta 3$ )	<sup>99m</sup> Tc-3PRGD <sub>2</sub> [70]	SPECT	<ul style="list-style-type: none"> <li>• Upregulated in angiogenesis and are involved with MMPs</li> <li>• Overexpression seen in aggressive tumors</li> </ul>



Table 2. Cont.

Radiolabeled Substance	Example Radiotracer	Tracer Modality *	Significance
Matrix metalloproteinases (MMP)	<sup>68</sup> Ga-DOTA-TCTP-1 (MMP-2) [71]	PET	<ul style="list-style-type: none"> <li>Involved in angiogenesis</li> <li>Degrades the basement membrane</li> <li>Permits branching</li> </ul>
Fibronectin	<sup>76</sup> Br-L19-SIP (ED-B) [72]	PET	<ul style="list-style-type: none"> <li>Absent in healthy adult tissue</li> <li>Found in neoplastic cells</li> </ul>
Nitroimidazole	<sup>18</sup> F-FETNIM [73]	PET	<ul style="list-style-type: none"> <li>Nitroimidazole is upregulated in hypoxic tissue</li> <li>Appears to play a role in angiogenesis</li> </ul>

\* The modality is dependent on the radiotracer used. Abbreviations: VEGF, vascular endothelial growth factor; VEGFR, vascular endothelial growth factor receptor; PET, positron emission tomography; SPECT, single-positron emission computer tomography; MMP, matrix metalloproteinases.

## 11. 18F-FDG- (Fluorine 18 Fluoro-Deoxy-Glucose)-Based Imaging

18F-FDG-based PET is the most frequently used radiotracer in the clinical setting. Its use in evaluating malignant lesions is dependent on the increased glucose metabolism in malignant tumor cells. However, its role in predicting tumor response to anti-angiogenic therapy is promising but not yet fully validated. Previously, a study revealed a strong association between tumor angiogenesis-related gene expression and 18F-FDG uptake [74]. There are several others which support this method, including a more recent study of renal cell carcinoma metastasis by Hwang et al. concluding that metabolic tumor volume and lesion glycolysis could provide prognostic information in patients treated with anti-VEGF therapy [15]. Investigations are ongoing to fully validate 18F-FDG PET in clinical use for evaluating tumor response to anti-angiogenic therapy.

### 11.1. VEGF and VEGFR Targeting

The targeting of VEGF or its tyrosine kinase receptor (VEGFR) via radiopharmaceuticals in PET or single-photon emission computerized tomography (SPECT) imaging is an exciting prospect. This technique may play an important role in the evaluation of anti-angiogenic treatment response since VEGFR-2 is upregulated in many neoplasms [75]. Preclinical studies reveal the possibility of radiopharmaceutical binding to VEGFR. This explains its role in imaging heterogeneity of tumor vasculature in animal breast cancer models and also its role in following up response to antiangiogenic drugs. However, these radiopharmaceutical agents must be refined for better understanding of their in vivo pharmacokinetics and to obtain a more potent affinity for VEGF [15].

### 11.2. Targeting Extracellular Matrix (ECM)

Fibronectin is an extracellular matrix protein that is expressed in normal tissues. Through alternative mRNA splicing, it can exist as an isoform that expresses an extra domain-B (ED-B). This isoform is found predominantly within fetal and neoplastic adult tissues and is often absent from healthy adult tissues. Malignant cells grow over a background of extracellular matrix proteins that expresses ED-B fibronectin. Thus, this isoform may be a potential target for molecular imaging evaluation of anti-angiogenic treatment response [76].

Other targets for radionuclide-based imaging include the integrins, predominantly alpha v beta 3, which are adhesive glycoproteins for extracellular matrix molecules. Both the alpha and beta subunits play an important role during angiogenesis, as they are upregulated in tumor metastasis to activate matrix metalloproteinase (MMP) that breaks down extracellular matrix [77]. Alpha v beta 3 overexpression is observed to be related to tumor aggressiveness and metastatic potentials. For example, Van Belle et al. discovered that these proteins are integral in advancing melanoma



transformation beyond radial superficial growth to deep vertical growth that denotes invasive pre-metastatic behavior [78].

### 11.3. Other Potential Targets

Matrix metalloproteinases (MMP) are a group of zinc-dependent proteolytic enzymes with both pro- and anti-angiogenic activities. They are released during angiogenesis to degrade cellular basement membranes and permit branching of newly formed blood vessels. Previously, MMP-2 has been successfully targeted and imaged in mouse models by attaching an MMP-2 inhibitor to Gallium-68, a radioisotope currently used in clinical practice [79]. These proteinases may serve as molecular targets for diagnostic and therapeutic interventions in the future [80].

Aminopeptidase N (APN) is a membrane-bound enzyme that is responsible for amino acid cleavage and has previously been shown to be involved in tumor angiogenesis [81]. Importantly, APN is absent within normal vasculature but has high expression within tumoral vessels undergoing angiogenesis [82]. This feature makes it a great target for evaluating angiogenesis activity within a tumor, and potentially for evaluating response to anti-angiogenesis agents. Studies have previously conjugated an APN-targeting agent to copper-68, a positron emitter used in PET, and technetium-99, an agent used in SPECT. Imaging was then performed and their utility demonstrated within mouse models [83,84].

## 12. Emerging Imaging Techniques for Angiogenesis

### 12.1. Ultrasound

Advances in ultrasound technology have introduced ultrafast techniques that deliver very high resolution and sensitivity. This allows for detailed characterization of the microvascular environment as well as quantification of blood flow without contrast [85]. Additionally, this technique has been shown to detect sluggish blood flow, as evidenced in rat models' microvasculature [11,86].

Ultrasound with contrast pulse sequences is a real-time perfusion imaging technique with a high specificity and spatial resolution. Multi-pulse contrast imaging suppresses linear back scattering from tissue (noise) while detecting a non-linear signal from the contrast agent (microbubbles). This allows for better assessment of small microvasculature where there is sluggish blood flow and a small concentration of microbubbles. In experimental studies, this technique produces results that are comparable to dynamic contrast-enhanced MRI in terms of perfusion parameters. In addition, contrast-enhanced ultrasound provides real-time imaging and detailed perfusion information during a single cardiac cycle [85].

### 12.2. Photoacoustic Imaging (PI)

Photoacoustic imaging is a relatively new advancement demonstrating promising results in clinical imaging. This technique utilizes optical waves (light) to vibrate a tissue, which then emits sonographic waves. A detector can then pick up the emitted wave and convert it to a usable image. There are several inherent advantages to this modality, including high-spatial and -temporal resolution and its ability to use endogenous substances as a contrast [87]. This includes hemoglobin, allowing the visualization of small vessels. Recently, a study performed using PI in prostate cancer patients found that imaging findings correlated well with areas of microvascular density and vascular area, suggesting a possible use in assessing prostate cancer angiogenesis [88]. Another study used PI to identify blood vessel densities in breast tissue with high resolution. With this, they were able to identify breast cancer lesions accurately [89]. Despite the many promises of photoacoustic imaging, there is still much work to be done before widespread clinical adoption, let alone validating it for use in follow-up of anti-angiogenesis treatment.

### 12.3. X-ray Phase Contrast Imaging

This is a new method which has not yet made its way into clinical imaging but has had several successes in the research and pre-clinical settings. Much like conventional radiography, this method uses ionizing X-rays, but instead of only measuring the degree of beam attenuation, it also accounts for beam distortion and scatter caused by the imaged structure. This results in an image with much improved resolution. An early study performed using both a phantom and a rat kidney found that CO<sub>2</sub> angiography resulted in a vessel resolution of around 60  $\mu\text{m}$  with simulations predicting a resolution of around 20  $\mu\text{m}$  in living tissue at reasonable radiation doses [90]. A follow-up study in a tumor model concluded that this method could be extended down to 15  $\mu\text{m}$  to allow for tumor angiogenesis analysis [91]. However, much like the above, there is significant work that needs to be done before clinical adoption.

## 13. Assessing the Response to Anti-Angiogenic Therapy

By using anti-angiogenic drugs, it is postulated that tumor vascular density will decrease more significantly than tumor cells density [92]. If the tumor cells regress faster than blood vessels, this in turn will increase the blood vessel index despite the decrease in tumor size; thus, the blood vessel index is rendered useless in evaluating anti-angiogenic response, giving a false impression of a stationary course [93].

Assessment of microvascular density in tissue biopsies is a straightforward, yet invasive, evaluation of therapy response [1]. However, the highest density of angiogenesis is found at the tumor periphery, while the core becomes de-vascularized and necrotic during tumor growth. Thus, obtaining comparable biopsies is challenging and could skew the observed response to treatment [31].

In summary, this review highlights various established and experimental methods for evaluating tumor response with anti-angiogenic therapy. While conventional imaging like CT, MRI, and US provide excellent anatomic characterization of tumor tissue, limited microvascular data are available. The addition of contrast agents to these conventional imaging modalities permits quantification of various perfusion parameters and provides insight on vascular function. Finally, molecular imaging utilizes a variety of targets to analyze anti-angiogenic therapy response on a microvascular level and provides a promising avenue for future advances. Regardless of the preferred imaging method, it is imperative to follow up anti-angiogenic treatment response. As these drugs pose many side effects to patients, it is essential to confirm a positive or negative therapeutic response to prevent the unnecessary continuation of these medications [21]. The use of anti-angiogenic factors also carries risk for thromboembolic events, mostly which result in myocardial infarction through switching the endothelial surface into a prothrombotic environment. Conversely, paradoxical bleeding is another complication that can be life threatening and difficult to manage, given the normal coagulation profile [94].

**Author Contributions:** Conceptualization of the manuscript: M.A.S., K.M.E.; Design and drafting of the manuscript: M.A.S., J.G., K.M.E.; Writing, editing, and revising the manuscript: J.G., A.M.R., A.E., A.W.M., A.D.K., S.K. and K.M.E. All authors have read and agreed to the published version of the manuscript.

**Funding:** This research received no external funding.

**Conflicts of Interest:** The authors declare no conflict of interest.

## References

1. Miller, J.C.; Pien, H.H.; Sahani, D.; Sorensen, A.G.; Thrall, J.H. Imaging angiogenesis: Applications and potential for drug development. *J. Natl. Cancer Inst.* **2005**, *97*, 172–187. [[CrossRef](#)]
2. Mulder, W.J.; Griffioen, A.W. Imaging of angiogenesis. *Angiogenesis* **2010**, *13*, 71–74. [[CrossRef](#)]
3. Abdalla, A.M.E.; Xiao, L.; Ullah, M.W.; Yu, M.; Ouyang, C.; Yang, G. Current Challenges of Cancer Anti-angiogenic Therapy and the Promise of Nanotherapeutics. *Theranostics* **2018**, *8*, 533–548. [[CrossRef](#)] [[PubMed](#)]

4. Zhang, J.; Xue, W.; Xu, K.; Yi, L.; Guo, Y.; Xie, T.; Tong, H.; Zhou, B.; Wang, S.; Li, Q.; et al. Dual inhibition of PFKFB3 and VEGF normalizes tumor vasculature, reduces lactate production, and improves chemotherapy in glioblastoma: Insights from protein expression profiling and MRI. *Theranostics* **2020**, *10*, 7245. [[CrossRef](#)]
5. Kallinowski, F.; Schlenger, K.H.; Runkel, S.; Kloes, M.; Stohrer, M.; Okunieff, P.; Vaupel, P. Blood flow, metabolism, cellular microenvironment, and growth rate of human tumor xenografts. *Cancer Res.* **1989**, *49*, 3759–3764.
6. Cai, W.; Chen, X. Multimodality molecular imaging of tumor angiogenesis. *J. Nucl. Med.* **2008**, *49*, 113S–128S. [[CrossRef](#)]
7. McDonald, D.M.; Choyke, P.L. Imaging of angiogenesis: From microscope to clinic. *Nat. Med.* **2003**, *9*, 713–725. [[CrossRef](#)]
8. Kong, Z.; Yan, C.; Zhu, R.; Wang, J.; Wang, Y.; Wang, Y.; Wang, R.; Feng, F.; Ma, W. Imaging biomarkers guided anti-angiogenic therapy for malignant gliomas. *Neuroimage Clin.* **2018**, *20*, 51–60. [[CrossRef](#)]
9. Raatschen, H.J.; Simon, G.H.; Fu, Y.; Sennino, B.; Shames, D.M.; Wendland, M.F.; McDonald, D.M.; Brasch, R.C. Vascular permeability during antiangiogenesis treatment: MR imaging assay results as biomarker for subsequent tumor growth in rats. *Radiology* **2008**, *247*, 391–399. [[CrossRef](#)]
10. Carmeliet, P.; Jain, R.K. Principles and mechanisms of vessel normalization for cancer and other angiogenic diseases. *Nat. Rev. Drug Discov.* **2011**, *10*, 417–427. [[CrossRef](#)]
11. Cao, Y.; Langer, R. A review of Judah Folkman's remarkable achievements in biomedicine. *Proc. Natl. Acad. Sci. USA* **2008**, *105*, 13203–13205. [[CrossRef](#)]
12. Demené, C.; Payen, T.; Dizeux, A.; Barrois, G.; Gennisson, J.; Bridal, L.; Tanter, M. 3-D Longitudinal Imaging of Tumor Angiogenesis in Mice in Vivo Using Ultrafast Doppler Tomography. *Ultrasound Med. Biol.* **2019**, *45*, 1284–1296. [[CrossRef](#)]
13. Rajabi, M.; Mousa, S.A. The Role of Angiogenesis in Cancer Treatment. *Biomedicines* **2017**, *5*, 34. [[CrossRef](#)] [[PubMed](#)]
14. Lugano, R.; Ramachandran, M.; Dimberg, A. Tumor angiogenesis: Causes, consequences, challenges and opportunities. *Cell. Mol. Life Sci.* **2020**, *77*, 1745–1770. [[CrossRef](#)]
15. Niccoli Asabella, A.; Di Palo, A.; Altini, C.; Ferrari, C.; Rubini, G. Multimodality Imaging in Tumor Angiogenesis: Present Status and Perspectives. *Int. J. Mol. Sci.* **2017**, *18*, 1864. [[CrossRef](#)] [[PubMed](#)]
16. Senger, D.R. Vascular endothelial growth factor: Much more than an angiogenesis factor. *Mol. Biol. Cell* **2010**, *21*, 377–379. [[CrossRef](#)]
17. Iagaru, A.; Gambhir, S.S. Imaging tumor angiogenesis: The road to clinical utility. *Am. J. Roentgenol.* **2013**, *201*, W183–W191. [[CrossRef](#)]
18. Bergers, G.; Benjamin, L.E. Tumorigenesis and the angiogenic switch. *Nat. Rev. Cancer* **2003**, *3*, 401–410. [[CrossRef](#)]
19. Jeswani, T.; Padhani, A.R. Imaging tumour angiogenesis. *Cancer Imaging* **2005**, *5*, 131–138. [[CrossRef](#)]
20. Giannotta, M.; Trani, M.; Dejana, E. VE-cadherin and endothelial adherens junctions: Active guardians of vascular integrity. *Dev. Cell* **2013**, *26*, 441–454. [[CrossRef](#)]
21. Garcia-Figueiras, R.; Goh, V.J.; Padhani, A.R.; Baleato-Gonzalez, S.; Garrido, M.; Leon, L.; Gómez-Caamaño, A. CT perfusion in oncologic imaging: A useful tool? *Am. J. Roentgenol.* **2013**, *200*, 8–19. [[CrossRef](#)]
22. Lanza, G.M.; Winter, P.M.; Caruthers, S.D.; Hughes, M.S.; Cyrus, T.; Marsh, J.N.; Neubauer, A.M.; Partlow, K.C.; Wickline, S.A. Nanomedicine opportunities for cardiovascular disease with perfluorocarbon nanoparticles. *Nanomedicine* **2006**, *1*, 321–329. [[CrossRef](#)]
23. Li, K.C.; Guccione, S.; Bednarski, M.D. Combined vascular targeted imaging and therapy: A paradigm for personalized treatment. *J. Cell. Biochem. Suppl.* **2002**, *39*, 65–71. [[CrossRef](#)] [[PubMed](#)]
24. Jain, R.; Gutierrez, J.; Narang, J.; Scarpace, L.; Schultz, L.R.; Lemke, N.; Patel, S.C.; Mikkelsen, T.; Rock, J.P. In vivo correlation of tumor blood volume and permeability with histologic and molecular angiogenic markers in gliomas. *Am. J. Neuroradiol.* **2011**, *32*, 388–394. [[CrossRef](#)]
25. Santarosa, C.; Castellano, A.; Conte, G.M.; Cadioli, M.; Iadanza, A.; Terreni, M.R.; Franzin, A.; Bello, L.; Caulo, M.; Falini, A.; et al. Dynamic contrast-enhanced and dynamic susceptibility contrast perfusion MR imaging for glioma grading: Preliminary comparison of vessel compartment and permeability parameters using hotspot and histogram analysis. *Eur. J. Radiol.* **2016**, *85*, 1147–1156. [[CrossRef](#)]

26. Hilario, A.; Hernandez-Lain, A.; Sepulveda, J.M.; Lagares, A.; Perez-Nuñez, A.; Ramos, A. Perfusion MRI grading diffuse gliomas: Impact of permeability parameters on molecular biomarkers and survival. *Neurocirugía* **2019**, *30*, 11–18. [[CrossRef](#)]
27. Kim, J.; Kim, E.; Euceda, L.R.; Meyer, D.E.; Langseth, K.; Bathen, T.F.; Moestue, S.A.; Huuse, E.M. Multiparametric characterization of response to anti-angiogenic therapy using USPIO contrast-enhanced MRI in combination with dynamic contrast-enhanced MRI. *J. Magn. Reson. Imaging* **2018**, *47*, 1589–1600. [[CrossRef](#)] [[PubMed](#)]
28. Cho, K.J. Carbon Dioxide Angiography: Scientific Principles and Practice. *Vasc. Spec. Int.* **2015**, *31*, 67–80. [[CrossRef](#)]
29. Gounis, M.J.; Lieber, B.B.; Webster, K.A.; Wakhloo, A.K. A novel angiographic methodology for the quantification of angiogenesis. *IEEE Trans. Biomed. Eng.* **2008**, *55*, 996–1003. [[CrossRef](#)] [[PubMed](#)]
30. Kather, J.N.; Marx, A.; Reyes-Aldasoro, C.C.; Schad, L.R.; Zöllner, F.G.; Weis, C.A. Continuous representation of tumor microvessel density and detection of angiogenic hotspots in histological whole-slide images. *Oncotarget* **2015**, *6*, 19163. [[CrossRef](#)]
31. Miles, K.A. Tumour angiogenesis and its relation to contrast enhancement on computed tomography: A review. *Eur. J. Radiol.* **1999**, *30*, 198–205. [[CrossRef](#)]
32. Anderson, H.; Price, P.; Blomley, M.; Leach, M.O.; Workman, P. Measuring changes in human tumour vasculature in response to therapy using functional imaging techniques. *Br. J. Cancer* **2001**, *85*, 1085–1093. [[CrossRef](#)]
33. Zormpas-Petridis, K.; Jerome, N.P.; Blackledge, M.D.; Carceller, F.; Poon, E.; Clarke, M.; McErlean, C.M.; Barone, G.; Koers, A.; Vaidya, S.J.; et al. MRI Imaging of the Hemodynamic Vasculature of Neuroblastoma Predicts Response to Antiangiogenic Treatment. *Cancer Res.* **2019**, *79*, 2978–2991. [[CrossRef](#)]
34. Naish, J.H.; McGrath, D.M.; Bains, L.J.; Passera, K.; Roberts, C.; Watson, Y.; Cheung, S.; Taylor, M.B.; Logue, J.P.; Buckley, D.L.; et al. Comparison of dynamic contrast-enhanced MRI and dynamic contrast-enhanced CT biomarkers in bladder cancer. *Magn. Reson. Med.* **2011**, *66*, 219–226. [[CrossRef](#)]
35. O'Connor, J.P.; Jackson, A.; Parker, G.J.; Jayson, G.C. DCE-MRI biomarkers in the clinical evaluation of antiangiogenic and vascular disrupting agents. *Br. J. Cancer* **2007**, *96*, 189–195. [[CrossRef](#)]
36. Anderson, H.L.; Yap, J.T.; Miller, M.P.; Robbins, A.; Jones, T.; Price, P.M. Assessment of pharmacodynamic vascular response in a phase I trial of combretastatin A4 phosphate. *J. Clin. Oncol. Off. J. Am. Soc. Clin. Oncol.* **2003**, *21*, 2823–2830. [[CrossRef](#)]
37. Krix, M.; Kiessling, F.; Vosseler, S.; Farhan, N.; Mueller, M.M.; Bohlen, P.; Fusenig, N.E.; Delorme, S. Sensitive noninvasive monitoring of tumor perfusion during antiangiogenic therapy by intermittent bolus-contrast power Doppler sonography. *Cancer Res.* **2003**, *63*, 8264–8270.
38. Barrett, T.; Brechbiel, M.; Bernardo, M.; Choyke, P.L. MRI of tumor angiogenesis. *J. Magn. Reson. Imaging* **2007**, *26*, 235–249. [[CrossRef](#)] [[PubMed](#)]
39. Silva, A.C.; Kim, S.G.; Garwood, M. Imaging blood flow in brain tumors using arterial spin labeling. *Magn. Reson. Med.* **2000**, *44*, 169–173. [[CrossRef](#)]
40. Williams, D.S. Quantitative perfusion imaging using arterial spin labeling. *Methods Mol. Med.* **2006**, *124*, 151–173.
41. Tempel, C.; Neeman, M. Spatial and temporal modulation of perfusion in the rat ovary measured by arterial spin labeling MRI. *J. Magn. Reson. Imaging* **1999**, *9*, 794–803. [[CrossRef](#)]
42. Boss, A.; Martirosian, P.; Schraml, C.; Clasen, S.; Fenchel, M.; Anastasiadis, A.; Claussen, C.D.; Pereira, P.L.; Schick, F. Morphological, contrast-enhanced and spin labeling perfusion imaging for monitoring of relapse after RF ablation of renal cell carcinomas. *Eur. Radiol.* **2006**, *16*, 1226–1236. [[CrossRef](#)] [[PubMed](#)]
43. Reijnders, K.; English, S.J.; Krishna, M.C.; Cook, J.A.; Sowers, A.L.; Mitchell, J.B.; Zhang, Y. Influence of body temperature on the BOLD effect in murine SCC tumors. *Magn. Reson. Med.* **2004**, *51*, 389–393. [[CrossRef](#)] [[PubMed](#)]
44. Doblaz, S.; He, T.; Saunders, D.; Pearson, J.; Hoyle, J.; Smith, N.; Lerner, M.; Towner, R.A. Glioma morphology and tumor-induced vascular alterations revealed in seven rodent glioma models by in vivo magnetic resonance imaging and angiography. *J. Magn. Reson. Imaging* **2010**, *32*, 267–275. [[CrossRef](#)]
45. Kim, S.H.; Lee, H.S.; Kang, B.J.; Song, B.J.; Kim, H.B.; Lee, H.; Jin, M.S.; Lee, A. Dynamic Contrast-Enhanced MRI Perfusion Parameters as Imaging Biomarkers of Angiogenesis. *PLoS ONE* **2016**, *11*, e0168632. [[CrossRef](#)]
46. Padhani, A.R.; Dzik-Jurasz, A. Perfusion MR imaging of extracranial tumor angiogenesis. *Top. Magn. Reson. Imaging* **2004**, *15*, 41–57. [[CrossRef](#)]

47. Provenzale, J.M.; Wang, G.R.; Brenner, T.; Petrella, J.R.; Sorensen, A.G. Comparison of permeability in high-grade and low-grade brain tumors using dynamic susceptibility contrast MR imaging. *Am. J. Roentgenol.* **2002**, *178*, 711–716. [[CrossRef](#)]
48. Zhang, J.; Liu, H.; Tong, H.; Wang, S.; Yang, Y.; Liu, G.; Zhang, W. Clinical applications of contrast-enhanced perfusion MRI techniques in gliomas: Recent advances and current challenges. *Contrast Media Mol. Imaging* **2017**, *2017*, 7064120. [[CrossRef](#)] [[PubMed](#)]
49. Choyke, P.L.; Dwyer, A.J.; Knopp, M.V. Functional tumor imaging with dynamic contrast-enhanced magnetic resonance imaging. *J. Magn. Reson. Imaging* **2003**, *17*, 509–520. [[CrossRef](#)]
50. Essig, M.; Shiroishi, M.S.; Nguyen, T.B.; Saake, M.; Provenzale, J.M.; Enterline, D.; Anzalone, N.; Dörfler, A.; Rovira, A.; Wintermark, M.; et al. Perfusion MRI: The five most frequently asked technical questions. *Am. J. Roentgenol.* **2013**, *200*, 24–34. [[CrossRef](#)]
51. Tofts, P.S. T1-weighted DCE imaging concepts: Modelling, acquisition and analysis. *Signal* **2010**, *500*, 400.
52. Murase, K. Efficient method for calculating kinetic parameters using T1-weighted dynamic contrast-enhanced magnetic resonance imaging. *Magn. Reson. Med. Off. J. Int. Soc. Magn. Reson. Med.* **2004**, *51*, 858–862. [[CrossRef](#)]
53. D'Assignies, G.; Couvelard, A.; Bahrami, S.; Vullierme, M.; Hammel, P.; Hentic, O.; Sauvanet, A.; Bedossa, P.; Ruzsniowski, P.; Vilgrain, V. Pancreatic endocrine tumors: Tumor blood flow assessed with perfusion CT reflects angiogenesis and correlates with prognostic factors. *Radiology* **2009**, *250*, 407–416. [[CrossRef](#)]
54. Xu, N.; Lei, Z.; Li, X.L.; Zhang, J.; Li, C.; Feng, G.Q.; Li, D.N.; Liu, J.Y.; Wei, Q.; Bian, T.T.; et al. Clinical study of tumor angiogenesis and perfusion imaging using multi-slice spiral computed tomography for breast cancer. *Asian Pac. J. Cancer Prev.* **2013**, *14*, 429–433. [[CrossRef](#)] [[PubMed](#)]
55. Sun, C.H.; Feng, S.; Xiao, P.; Peng, Z.P.; Pui, M.H.; Li, X.H.; Li, Z.P.; Meng, Q.F. Quantitative assessment of perirectal tumor infiltration with dynamic contrast-enhanced multi-detector row CT in rectal cancer. *Eur. J. Radiol.* **2011**, *80*, 279–283. [[CrossRef](#)]
56. Mazzei, F.G.; Mazzei, M.A.; Cioffi Squitieri, N.; Pozzessere, C.; Righi, L.; Cirigliano, A.; Guerrini, S.; D'Elia, D.; Ambrosio, M.R.; Barone, A.; et al. CT perfusion in the characterisation of renal lesions: An added value to multiphasic CT. *BioMed Res. Int.* **2014**, *2014*, 135013. [[CrossRef](#)]
57. Trojanowska, A.; Trojanowski, P.; Bisdas, S.; Staśkiewicz, G.; Drop, A.; Klatka, J.; Bobek-Billewicz, B. Squamous cell cancer of hypopharynx and larynx—Evaluation of metastatic nodal disease based on computed tomography perfusion studies. *Eur. J. Radiol.* **2012**, *81*, 1034–1039. [[CrossRef](#)] [[PubMed](#)]
58. Liu, Y.; Bellomi, M.; Gatti, G.; Ping, X. Accuracy of computed tomography perfusion in assessing metastatic involvement of enlarged axillary lymph nodes in patients with breast cancer. *Breast Cancer Res.* **2007**, *9*, R40. [[CrossRef](#)]
59. Carmeliet, P.; Jain, R.K. Angiogenesis in cancer and other diseases. *Nature* **2000**, *407*, 249–257. [[CrossRef](#)]
60. Ehling, J.; Lammers, T.; Kiessling, F. Non-invasive imaging for studying anti-angiogenic therapy effects. *Thromb. Haemost.* **2013**, *109*, 375–390. [[CrossRef](#)]
61. Jugold, M.; Palmowski, M.; Huppert, J.; Woenne, E.C.; Mueller, M.M.; Semmler, W.; Kiessling, F. Volumetric high-frequency Doppler ultrasound enables the assessment of early antiangiogenic therapy effects on tumor xenografts in nude mice. *Eur. Radiol.* **2008**, *18*, 753–758. [[CrossRef](#)]
62. Goodwin, A.P.; Nakatsuka, M.A.; Mattrey, R.F. Stimulus-responsive ultrasound contrast agents for clinical imaging: Motivations, demonstrations, and future directions. *Wiley Interdiscip. Rev. Nanomed. Nanobiotechnol.* **2015**, *7*, 111–123. [[CrossRef](#)]
63. Kiessling, F.; Huppert, J.; Palmowski, M. Functional and molecular ultrasound imaging: Concepts and contrast agents. *Curr. Med. Chem.* **2009**, *16*, 627–642. [[CrossRef](#)] [[PubMed](#)]
64. Sirsi, S.R.; Flexman, M.L.; Vlachos, F.; Huang, J.; Hernandez, S.L.; Kim, H.K.; Johung, T.B.; Gander, J.W.; Reichstein, A.R.; Lampl, B.S.; et al. Contrast ultrasound imaging for identification of early responder tumor models to anti-angiogenic therapy. *Ultrasound Med. Biol.* **2012**, *38*, 1019–1029. [[CrossRef](#)]
65. Pysz, M.A.; Foygel, K.; Rosenberg, J.; Gambhir, S.S.; Schneider, M.; Willmann, J.K. Antiangiogenic cancer therapy: Monitoring with molecular US and a clinically translatable contrast agent (BR55). *Radiology* **2010**, *256*, 519–527. [[CrossRef](#)]
66. Niu, G.; Chen, X. PET Imaging of Angiogenesis. *PET Clin.* **2009**, *4*, 17–38. [[CrossRef](#)]
67. O'Connor, J.P.B. Imaging angiogenesis: Role in measuring response to treatment. *Antiangiogenesis Cancer Ther.* **2014**, 29–48. [[CrossRef](#)]



68. Hu, K.; Shang, J.; Xie, L.; Hanyu, M.; Zhang, Y.; Yang, Z.; Xu, H.; Wang, L.; Zhang, M.R. PET Imaging of VEGFR with a Novel <sup>64</sup>Cu-Labeled Peptide. *ACS Omega* **2020**, *5*, 8508–8514. [[CrossRef](#)] [[PubMed](#)]
69. Jansen, M.H.; Lagerweij, T.; Sewing, A.C.; Vugts, D.J.; van Vuurden, D.G.; Molthoff, C.F.; Caretti, V.; Veringa, S.J.; Petersen, N.; Carcaboso, A.M.; et al. Bevacizumab Targeting Diffuse Intrinsic Pontine Glioma: Results of <sup>89</sup>Zr-Bevacizumab PET Imaging in Brain Tumor Models. *Mol. Cancer Ther.* **2016**, *15*, 2166–2174. [[CrossRef](#)]
70. Zhu, Z.; Miao, W.; Li, Q.; Dai, H.; Ma, Q.; Wang, F.; Yang, A.; Jia, B.; Jing, X.; Liu, S.; et al. <sup>99m</sup>Tc-3PRGD2 for integrin receptor imaging of lung cancer: A multicenter study. *J. Nucl. Med.* **2012**, *53*, 716–722. [[CrossRef](#)]
71. Kiugel, M.; Hellberg, S.; Käkälä, M.; Liljenbäck, H.; Saanijoki, T.; Li, X.G.; Tuomela, J.; Knuuti, J.; Saraste, A.; Roivainen, A. Evaluation of [<sup>68</sup>Ga]Ga-DOTA-TCTP-1 for the Detection of Metalloproteinase 2/9 Expression in Mouse Atherosclerotic Plaques. *Molecules* **2018**, *23*, 3168. [[CrossRef](#)]
72. Rossin, R.; Berndorff, D.; Friebe, M.; Dinkelborg, L.M.; Welch, M.J. Small-animal PET of tumor angiogenesis using a (76)Br-labeled human recombinant antibody fragment to the ED-B domain of fibronectin. *J. Nucl. Med.* **2007**, *48*, 1172–1179. [[CrossRef](#)] [[PubMed](#)]
73. Hu, M.; Zhu, Y.; Mu, D.; Fan, B.; Zhao, S.; Yang, G.; Ma, L.; Zheng, J.; Yu, J. Correlation of hypoxia as measured by fluorine-18 fluoroerythronitroimidazole (18F-FETNIM) PET/CT and overall survival in glioma patients. *Eur. J. Nucl. Med. Mol. Imaging* **2020**, *47*, 1427–1434. [[CrossRef](#)] [[PubMed](#)]
74. Strauss, L.G.; Koczan, D.; Klippel, S.; Pan, L.; Cheng, C.; Willis, S.; Haberkorn, U.; Dimitrakopoulou-Strauss, A. Impact of angiogenesis-related gene expression on the tracer kinetics of 18F-FDG in colorectal tumors. *J. Nucl. Med.* **2008**, *49*, 1238–1244. [[CrossRef](#)]
75. Ferrara, N. Vascular endothelial growth factor: Basic science and clinical progress. *Endocr. Rev.* **2004**, *25*, 581–611. [[CrossRef](#)]
76. Borsi, L.; Balza, E.; Bestagno, M.; Castellani, P.; Carnemolla, B.; Biro, A.; Leprini, A.; Sepulveda, J.; Burrone, O.; Neri, D.; et al. Selective targeting of tumoral vasculature: Comparison of different formats of an antibody (L19) to the ED-B domain of fibronectin. *Int. J. Cancer J. Int. Cancer* **2002**, *102*, 75–85. [[CrossRef](#)] [[PubMed](#)]
77. Hood, J.D.; Cheresch, D.A. Role of integrins in cell invasion and migration. *Nat. Rev. Cancer* **2002**, *2*, 91–100. [[CrossRef](#)]
78. Van Belle, P.A.; Elenitsas, R.; Satyamoorthy, K.; Wolfe, J.T.; Guerry, D.; Schuchter, L.; van Belle, T.J.; Albelda, S.; Tahin, P.; Herlyn, M.; et al. Progression-related expression of beta3 integrin in melanomas and nevi. *Hum. Pathol.* **1999**, *30*, 562–567. [[CrossRef](#)]
79. Liu, Q.; Pan, D.; Cheng, C.; Zhang, A.; Ma, C.; Wang, L.; Zhang, D.; Liu, H.; Jiang, H.; Wang, T.; et al. Targeting of MMP2 activity in malignant tumors with a <sup>68</sup>Ga-labeled gelatinase inhibitor cyclic peptide. *Nucl. Med. Biol.* **2015**, *42*, 939–944. [[CrossRef](#)]
80. Matter, A. Tumor angiogenesis as a therapeutic target. *Drug Discov. Today* **2001**, *6*, 1005–1024. [[CrossRef](#)]
81. Bhagwat, S.V.; Lahdenranta, J.; Giordano, R.; Arap, W.; Pasqualini, R.; Shapiro, L.H. CD13/APN is activated by angiogenic signals and is essential for capillary tube formation. *Blood* **2001**, *97*, 652–659. [[CrossRef](#)]
82. Pasqualini, R.; Koivunen, E.; Kain, R.; Lahdenranta, J.; Sakamoto, M.; Stryhn, A.; Ashmun, R.A.; Shapiro, L.H.; Arap, W.; Ruoslahti, E. Aminopeptidase N is a receptor for tumor-homing peptides and a target for inhibiting angiogenesis. *Cancer Res.* **2000**, *60*, 722–727.
83. Chen, K.; Ma, W.; Li, G.; Wang, J.; Yang, W.; Yap, L.P.; Hughes, L.D.; Park, R.; Conti, P.S. Synthesis and evaluation of <sup>64</sup>Cu-labeled monomeric and dimeric NGR peptides for MicroPET imaging of CD13 receptor expression. *Mol. Pharm.* **2013**, *10*, 417–427. [[CrossRef](#)]
84. Ma, W.; Kang, F.; Wang, Z.; Yang, W.; Li, G.; Ma, X.; Li, G.; Chen, K.; Zhang, Y.; Wang, J. (<sup>99m</sup>Tc)-labeled monomeric and dimeric NGR peptides for SPECT imaging of CD13 receptor in tumor-bearing mice. *Amino Acids* **2013**, *44*, 1337–1345. [[CrossRef](#)]
85. Leow, C.H.; Bush, N.L.; Stanzola, A.; Braga, M.; Shah, A.; Hernandez-Gil, J.; Long, N.J.; Aboagye, E.O.; Bamber, J.C.; Tang, M.X. 3-D Microvascular Imaging Using High Frame Rate Ultrasound and ASAP without Contrast Agents: Development and Initial In Vivo Evaluation on Nontumor and Tumor Models. *IEEE Trans. Ultrason. Ferroelectr. Freq. Control* **2019**, *66*, 939–948. [[CrossRef](#)]
86. Rissanen, T.T.; Korpisalo, P.; Karvinen, H.; Liimatainen, T.; Laidinen, S.; Grohn, O.H.; Ylä-Herttuala, S. High-resolution ultrasound perfusion imaging of therapeutic angiogenesis. *JACC Cardiovasc. Imaging* **2008**, *1*, 83–91. [[CrossRef](#)]

87. Steinberg, I.; Huland, D.M.; Vermesh, O.; Frostig, H.E.; Tummers, W.S.; Gambhir, S.S. Photoacoustic clinical imaging. *Photoacoustics* **2019**, *14*, 77–98. [[CrossRef](#)]
88. Horiguchi, A.; Shinchu, M.; Nakamura, A.; Wada, T.; Ito, K.; Asano, T.; Shinmoto, H.; Tsuda, H.; Ishihara, M. Pilot Study of Prostate Cancer Angiogenesis Imaging Using a Photoacoustic Imaging System. *Urology* **2017**, *108*, 212–219. [[CrossRef](#)] [[PubMed](#)]
89. Lin, L.; Hu, P.; Shi, J.; Appleton, C.M.; Maslov, K.; Li, L.; Zhang, R.; Wang, L.V. Single-breath-hold photoacoustic computed tomography of the breast. *Nat. Commun.* **2018**, *9*, 2352. [[CrossRef](#)]
90. Lundström, U.; Larsson, D.H.; Burvall, A.; Takman, P.A.; Scott, L.; Brismar, H.; Hertz, H.M. X-ray phase contrast for CO<sub>2</sub> microangiography. *Phys. Med. Biol.* **2012**, *57*, 2603–2617. [[CrossRef](#)]
91. Lundström, U.; Westermark, U.K.; Larsson, D.H.; Burvall, A.; Arsenian Henriksson, M.; Hertz, H.M. X-ray phase contrast with injected gas for tumor microangiography. *Phys. Med. Biol.* **2014**, *59*, 2801–2811. [[CrossRef](#)]
92. Zhang, W.; Ran, S.; Sambade, M.; Huang, X.; Thorpe, P.E. A monoclonal antibody that blocks VEGF binding to VEGFR2 (KDR/Flk-1) inhibits vascular expression of Flk-1 and tumor growth in an orthotopic human breast cancer model. *Angiogenesis* **2002**, *5*, 35–44. [[CrossRef](#)]
93. Hlatky, L.; Hahnfeldt, P.; Folkman, J. Clinical Application of Antiangiogenic Therapy: Microvessel Density, What It Does and Doesn't Tell Us. *J. Natl. Cancer Inst.* **2002**, *94*, 883–893. [[CrossRef](#)]
94. Elice, F.; Rodeghiero, F.; Falanga, A.; Rickles, F.R. Thrombosis associated with angiogenesis inhibitors. *Best Pract. Res. Clin. Haematol.* **2009**, *22*, 115–128. [[CrossRef](#)]

**Publisher's Note:** MDPI stays neutral with regard to jurisdictional claims in published maps and institutional affiliations.



© 2020 by the authors. Licensee MDPI, Basel, Switzerland. This article is an open access article distributed under the terms and conditions of the Creative Commons Attribution (CC BY) license (<http://creativecommons.org/licenses/by/4.0/>).